Materials Research Letters

ISSN: 2166-3831 (Online) Journal homepage: www.tandfonline.com/journals/tmrl20

# A strategy to improve the work-hardening behavior of Ti–6Al–4V parts produced by additive manufacturing

**Charlotte de Formanoir, Alice Brulard, Solange Vivès, Guilhem Martin, Frédéric Prima, Sébastien Michotte, Edouard Rivière, Adrien Dolimont & Stéphane Godet**

**To cite this article:** Charlotte de Formanoir, Alice Brulard, Solange Vivès, Guilhem Martin, Frédéric Prima, Sébastien Michotte, Edouard Rivière, Adrien Dolimont & Stéphane Godet (2017) A strategy to improve the work-hardening behavior of Ti–6Al–4V parts produced by additive manufacturing, Materials Research Letters, 5:3, 201-208, DOI: 10.1080/21663831.2016.1245681

**To link to this article:** https://doi.org/10.1080/21663831.2016.1245681

© 2016 The Author(s). Published by Informa UK Limited, trading as Taylor & Francis Group.

Published online: 24 Oct 2016.

Submit your article to this journal

Article views: 8076

View related articles

View Crossmark data

Citing articles: 48 View citing articles

Full Terms & Conditions of access and use can be found at
https://www.tandfonline.com/action/journalInformation?journalCode=tmrl20

MATER. RES. LETT., 2017
VOL. 5, NO. 3, 201–208
http://dx.doi.org/10.1080/21663831.2016.1245681

MATERIALS RESEARCH LETTERS
Taylor & Francis
Taylor & Francis Group

ORIGINAL REPORT

OPEN ACCESS

# A strategy to improve the work-hardening behavior of Ti–6Al–4V parts produced by additive manufacturing

Charlotte de Formanoir[a], Alice Brulard[a], Solange Vivès[a], Guilhem Martin[b,c], Frédéric Prima[d], Sébastien Michotte[e], Edouard Rivière[f], Adrien Dolimont[f] and Stéphane Godet[a]

[a]4MAT, Université Libre de Bruxelles, Bruxelles, Belgium; [b]SIMaP, Université Grenoble Alpes, Grenoble, France; [c]SIMaP, CNRS, Grenoble, France; [d]Chimie ParisTech – CNRS, Institut de Recherche de Chimie Paris, PSL Research University, Paris, France; [e]T-ADD, Sirris, Gosselies, Belgium; [f]Machine Design and Production Engineering Unit, Faculty of Engineering, Université de Mons, Mons, Belgium

**ABSTRACT**

To improve the mechanical properties of additively manufactured parts, specific heat treatments must be developed. Annealing of electron beam-melted Ti–6Al–4V was performed at sub-transus temperatures and followed by water quenching. Such treatments generate an $\alpha+\alpha'$ dual-phase microstructure. Microstructural and mechanical characterizations revealed that the heat-treated specimens show a broad range of tensile properties, depending on the fraction of martensite. The specimens treated between 850°C and 920°C exhibit an increase in strength and ductility, which is related to a remarkable hardening behavior. Work-hardening is attributed to kinematic hardening arising from the mechanical contrast between the $\alpha$ and $\alpha'$ phases.

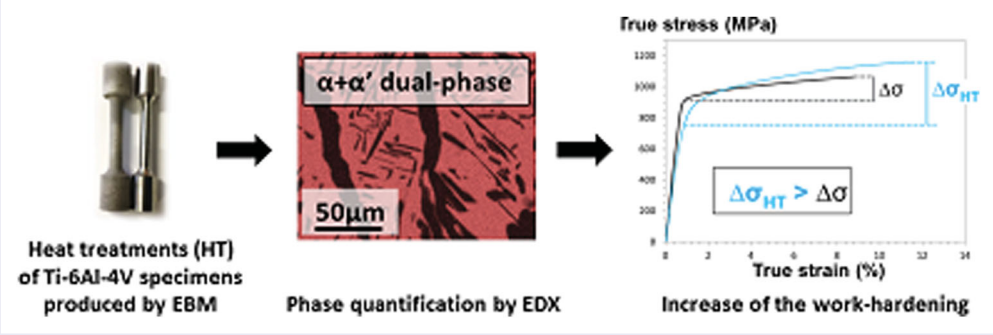


**ARTICLE HISTORY**
Received 27 July 2016

**KEYWORDS**
Additive manufacturing; Ti alloys; work-hardening; dual phases

**IMPACT STATEMENT**

Innovative heat treatments leading to $\alpha+\alpha'$ dual-phase microstructures are developed on Ti–6Al–4V parts produced by additive manufacturing. They lead to unprecedented work-hardening capabilities for this alloy.

## 1. Introduction

Ti–6Al–4V is an $\alpha+\beta$ titanium alloy showing a high strength-to-density ratio and biocompatibility. This makes it an excellent candidate for both aerospace and biomedical applications. In wrought Ti–6Al–4V, equiaxed or bimodal microstructures—obtained through complex multistep thermo-mechanical paths including hot deformation in the $\alpha+\beta$ field [1]—exhibit good ductility and fatigue strength [2]. However, low work-hardening rates are always reported, which is a major drawback for several industrial applications, including that in the aeronautical sector [3].

Additive manufacturing (AM) offers the opportunity to produce parts with complex geometries. However, the as-built Ti–6Al–4V microstructures obtained after AM substantially differ from those observed in the wrought conditions. Ti–6Al–4V produced by Selective Laser Melting (SLM) or Electron Beam Melting (EBM) typically exhibits a columnar morphology caused by the homoepitaxial growth of the parent $\beta$ grains during the solidification of the melt pool [4–10]. The microstructure resulting from the $\beta$ to $\alpha$ phase transformation is lamellar. In the case of SLM, the presence of acicular $\alpha'$ martensite is systematically reported [11–13], as a result of the

**CONTACT** Charlotte de Formanoir cdeforma@ulb.ac.be 4MAT, Université Libre de Bruxelles, 50 av. F.D. Roosevelt (CP 165/63), 1050 Bruxelles, Belgium

© 2016 The Author(s). Published by Informa UK Limited, trading as Taylor & Francis Group.
This is an Open Access article distributed under the terms of the Creative Commons Attribution License (http://creativecommons.org/licenses/by/4.0/), which permits unrestricted use, distribution, and reproduction in any medium, provided the original work is properly cited.

**Table 1.** Chemical composition of the ARCAM Ti–6Al–4V powder used in the EBM process.

| | Al | V | C | Fe | O | N | H | Ti |
|---|---|---|---|---|---|---|---|---|
| Arcam Ti–6Al–4V | 6% | 4% | 0.03% | 0.10% | 0.15% | 0.01% | 0.003% | Balance |

fast cooling rate. This fully martensitic microstructure is detrimental to the ductility [14]. However, for the EBM process, a fine $\alpha + \beta$ basket-weave microstructure is typically observed [4,5]. The resulting ductility of EBM parts, although higher than that of SLM parts, remains lower than that obtained in conventional wrought materials [15]. Indeed, the microstructure optimization of wrought Ti–6Al–4V typically involves hot working in the $(\alpha + \beta)$ phase field [1]. This allows the development of equiaxed or duplex/bimodal microstructures, resulting in a good balance between strength and ductility. However, in Ti–6Al–4V produced by *near-net shape* manufacturing processes, such as EBM, such thermo-mechanical pathways for microstructural optimization are excluded and, therefore, the formation of lamellar morphologies during the process cannot be avoided. Besides, in AM, the post-treatments for microstructural optimization are limited to pure thermal processing. As a consequence, specific thermal pathways still have to be developed for AM parts in order to substantially improve their mechanical properties without altering their as-built geometry. Several types of thermal posttreatments have been investigated in SLM parts [13,16]. They mainly aim at eliminating residual stresses and transforming the martensitic structure into the usual $\alpha + \beta$ structure. However, thermal posttreatments performed on EBM parts remain poorly documented. Besides, those reported so far only induce marginal improvements of the mechanical properties of EBM-parts [10]. In particular, they do not result in a significant enhancement of the balance between strength and ductility, and work-hardening remains very limited [10].

In this paper, post-EBM heat treatments, specifically designed for generating $\alpha/\alpha'$ dual-phase microstructures, are suggested and investigated. The resulting work-hardening behavior and strength/ductility balance obtained for various $\alpha/\alpha'$ phase fractions are illustrated and discussed.

## 2. Experimental procedure

Cylindrical tensile specimens were manufactured by EBM using an Arcam AB® A2 machine, with the standard ARCAM melting parameters, and a layer thickness of 70 µm (see e.g. [10] for more information regarding the process parameters). The chemical composition of the Ti–6Al–4V powder used to build these parts is reported in Table 1. The uniform section of these specimens was 30 mm in length and 5.5 mm in diameter.

The characterization of the intrinsic material properties required the removal of all macroscopic defects from both the bulk and the surface of the parts. It is indeed well known that those defects significantly decrease the ductility of parts produced by EBM [10,17]. To reduce the amount of critical defects in the bulk, the specimens were first submitted to Hot Isostatic Pressing (HIP)—that is, 2 h under a pressure of 1000 bar at 920°C followed by a slow furnace cooling—[14,18]. After HIP, the surface defects were removed by machining (reduction of the diameter from 5.5 mm to 4.5 mm). Each sample was then submitted to a specific heat treatment. The tensile specimens were first placed in a quartz capsule, under a protective argon atmosphere, to avoid oxidation and oxygen contamination. Heat treatments were performed for 2 h at sub-transus temperatures ranging from 850°C to 980°C in order to obtain different proportions of $\alpha/\beta$ [19]. To ensure the transformation of the $\beta$ phase into $\alpha'$ martensite, water quenching (WQ) was applied after breaking the quartz tube at the end of the isothermal annealing. For each annealing temperature, three specimens were heat treated and water quenched. Tensile testing was then carried out at room temperature to fracture and the strain was measured with an extensometer at a cross-head speed of 1 mm/min. The microstructures were characterized by SEM, XRD (X'Pert Pro by PANalytical, Cu K$\alpha$ radiation, scan step of 0.017°, counting time of 4 s) and EDX analyses. Each EDX scan (typically 100 µm by 100 µm) represents an acquisition time of 8 h, and for each annealing temperature, three scans were performed.

## 3. Results and discussions

HIP-underwent specimens that did not undergo any further posttreatment exhibit an $\alpha+\beta$ lamellar microstructure (Figure 1(a)). The $\alpha$ lamellae are significantly coarser (3–4 µm) than that in as-built electron beam melted parts (about 1 µm). The amount of $\beta$ is also increased by the HIP treatment. This coarse $\alpha + \beta$ microstructure has already been observed, see for example [4,18], and was attributed to the relatively slow cooling rate applied to the material after HIP. Heat-treated specimens exhibit a different microstructure, as reported in Figure 1(b–f). Fine $\alpha$ lamellae coexist with much thinner laths, which exhibit an acicular morphology that is characteristic of

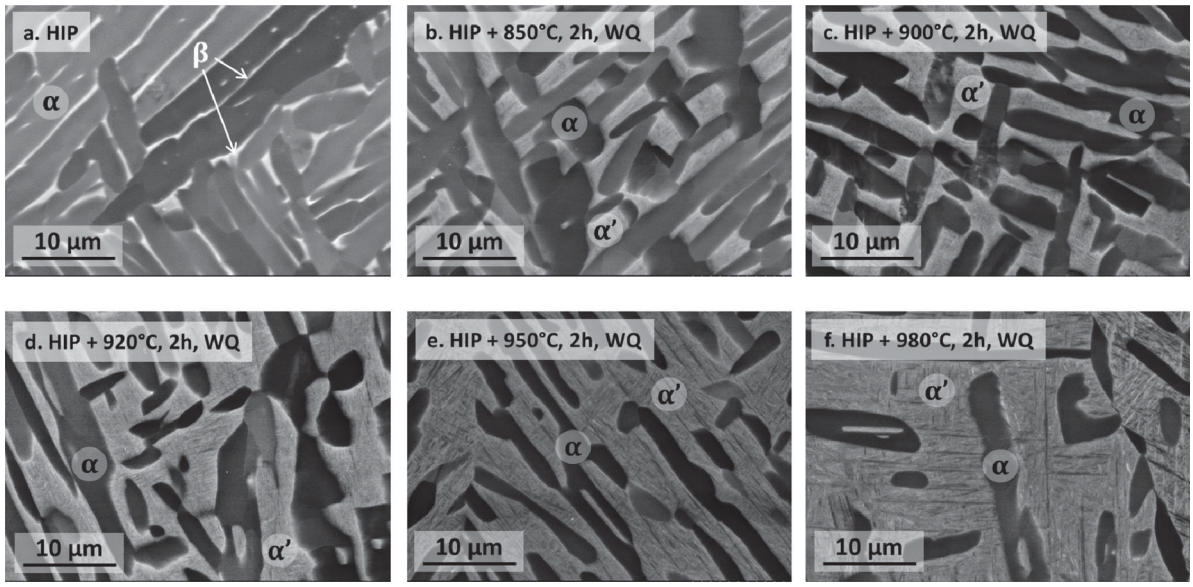


**Figure 1.** SEM micrographs of HIP-underwent and heat-treated specimens (BSE contrast): (a) HIP-underwent; (b) HIP + 850°C, 2 h, water quenched; (c) HIP + 900°C, 2 h, water quenched; (d) HIP + 920°C, 2 h, water quenched; (e) HIP + 950°C, 2 h, water quenched; and (f) HIP + 980°C, 2 h, water quenched.

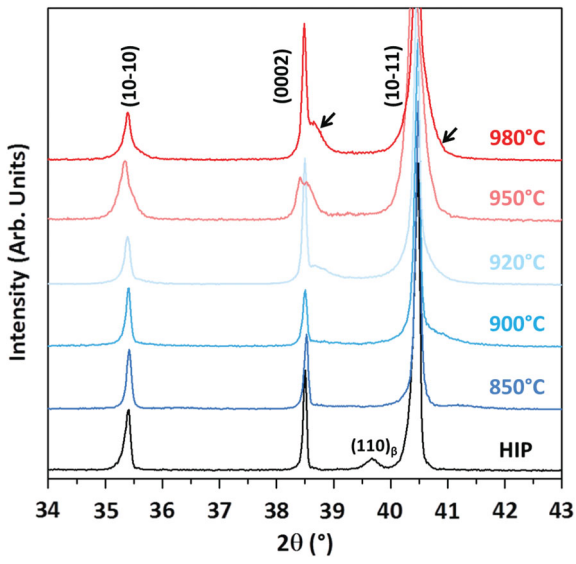


**Figure 2.** XRD profile of the heat-treated and HIP-underwent specimens. The arrows highlight splitting of the (0002) peak and broadening of the [10,11] peak, which reveal the presence of $\alpha'$-martensite in the heat-treated specimens.

$\alpha'$ martensite. The amount of $\alpha$ lamellae decreases as the annealing temperature increases, whereas larger fractions of $\alpha'$ laths can be observed.

The presence of martensite in the microstructure of the heat-treated and water-quenched samples was confirmed by the XRD analysis. As highlighted in Figure 2, splitting and broadening of some peaks can be observed in the XRD pattern of the heat-treated specimens. As previously observed in [20], this demonstrates the presence of a metastable $\alpha'$ phase along with the equilibrium $\alpha$ phase. Indeed, the $\alpha'$ phase exhibits a different chemical composition and therefore slightly different lattice parameters. The presence of $\alpha'$ martensite is particularly visible in the XRD patterns of specimens treated at high annealing temperatures, which exhibit higher fractions of $\alpha'$.

It should also be noted that the absence of $\beta$ peak in the XRD patterns of the heat-treated and water-quenched samples confirms that the volume fraction of remaining $\beta$ in these specimens is very low and/or that the $\beta$ is too fine to be detected. This is not the case for the, HIP-underwent specimens for which a $\beta$ peak can clearly be observed.

The dual $\alpha + \alpha'$ microstructure observed in the heat-treated and water-quenched specimens results from fast cooling of the $\alpha + \beta$ field. Quenching of the $\beta$ phase leads to the formation of martensite. Increasing the annealing temperature leads to a higher fraction of $\beta$ and therefore to larger fractions of martensite.

The fraction of martensite was measured by the image analysis based on EDX V- and Al-element maps. In Figure 3(a), the V-enriched phase and the Al-enriched phase are highlighted in red and blue, respectively. Vanadium, a $\beta$ stabilizer, is well known to partition preferentially to the $\beta$ phase during annealing treatments carried out in the $\alpha + \beta$ temperature range [3]. Consequently, the V concentration should be larger in the $\alpha'$ phase resulting from a fast cooling of the $\beta$ phase. On the other hand, Al is known to be an $\alpha$ stabilizer, and will therefore be present in larger amounts in the

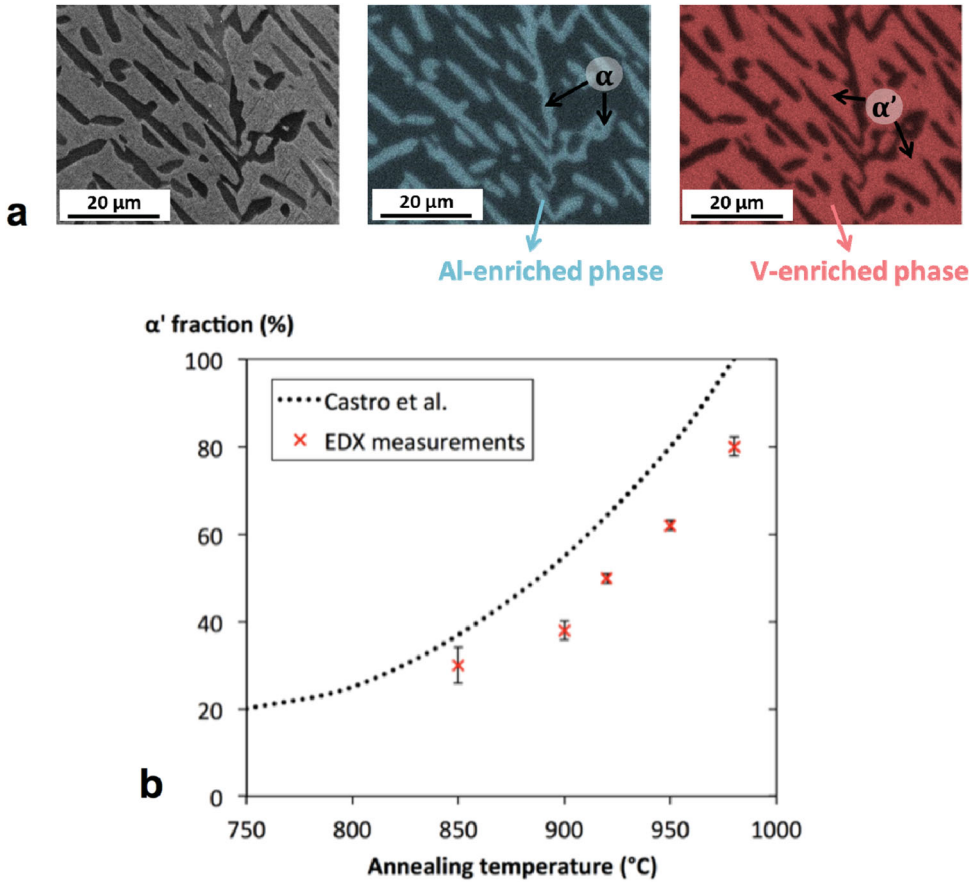


**Figure 3.** (a) SEM micrograph (BSE contrast), and corresponding EDX Al- and V-element maps on a specimen treated for 2 h at 950°C and water quenched; (b) martensite fraction as a function of the annealing temperature. The results obtained by Castro et al. [19] are also reported (dotted line).

$\alpha$ phase [3]. This partition of V and Al in the $\alpha'$ and $\alpha$ phases was recently reported by Tan et al. [21]. It has to be stressed that, although EDX does not provide a quantitative measurement of the element concentration in each phase, the difference in composition between the $\alpha$ and $\alpha'$ phases gives sufficient contrast so as to allow a semi-quantitative evaluation of the volume fraction of each phase. The martensite fraction is plotted as a function of the annealing temperature in Figure 3(b). Those results are relatively consistent with those published in [19]. The difference between the two curves can be attributed to the lower transus temperature reported by Castro et al. in [19], namely 980°C. In comparison, the material used in this work had a transus temperature of $995 \pm 5$°C, which might result from a slightly higher amount of $\alpha$-stabilizers in its composition.

Depending on the annealing temperature, the tensile behavior varies significantly in terms of strength and ductility. The true stress–strain curves up to necking are reported in Figure 4(a). The work-hardening behavior described by $n_{\text{incr}} = \mathrm{d}\ln\sigma/\mathrm{d}\ln\varepsilon$ is plotted in Figure 4(b). The average yield strength, engineering ultimate tensile strength, maximum true strength and uniform engineering elongation are reported in Table 2 for each annealing temperature, along with the corresponding fraction of $\alpha'$ martensite. In order to quantify the strain to failure, the reduction of area was also measured and reported in Table 2. It should be highlighted that, depending on the annealing temperature, a broad range of mechanical properties is achieved.

HIP-underwent specimens exhibit a relatively high yield strength but a moderate ductility. This can be attributed to their very low work-hardening capabilities. A typical stress–strain curve obtained on a wrought sample is also presented for a comparison. It exhibits a lower yield strength and larger uniform elongation. Its work-hardening is also very limited. On the contrary, all the heat treatments performed in this work induce a much higher work-hardening. $\Delta\sigma$, defined as the difference between the maximum true strength and the yield strength, is indeed two to three times larger than in the HIP-underwent or wrought specimens. Annealing

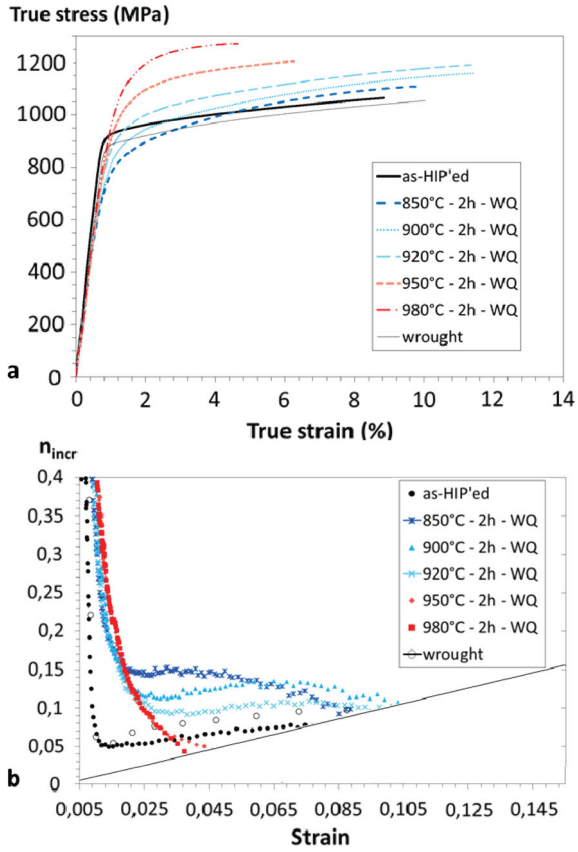


**Figure 4.** (a) True stress–true strain curves until necking and (b) work-hardening exponent $n_{\text{incr}}$ as a function of the strain for tensile specimens manufactured by EBM, HIP-underwent and heat-treated. Intersection with the straight line occurs when the Considere's criterion for the onset of necking is fulfilled, that is when the strain is equal to $n_{\text{incr}}$.

temperatures of 920°C, 900°C and 850°C lead to high ultimate tensile strength (as a result of significant work hardening) combined with a uniform strain and a reduction of area higher than those of HIP-underwent specimens. At 950°C, intermediate properties are achieved: in comparison to the HIP-underwent specimens, the uniform strain is lower, but the reduction of area is slightly improved. Finally, the specimens treated at 980°C exhibit the highest yield strength and ultimate tensile strength, but a very low ductility, which is consistent with a high volume fraction of $\alpha'$ martensite.

These observations are further illustrated in Figure 5, which highlights the remarkable improvement in both strength and ductility observed in the specimens treated at a temperature between 850°C and 920°C, compared to the as-built and HIP-underwent specimens. As for those treated at 980°C and 950°C, they exhibit a very high yield strength which comes along with a lower ductility.

Figure 4(b) shows the evolution of the work-hardening coefficient $n_{\text{incr}}$ as a function of strain and annealing temperature. The wrought sample and the EBM and HIP-underwent one exhibit similar work-hardening behaviors at the beginning of straining since their microstructure consists of both $\alpha$ and $\beta$ phases. The bimodal structure of the wrought sample enables larger hardening rates to be reached at larger strain levels, therefore leading to larger uniform elongation levels. For the samples heated at high temperatures (980°C and 950°C), even if the $n_{\text{incr}}$ is initially higher than that in the reference material, it decreases steeply so that Considere's criterion for the onset of necking is fulfilled at low strain levels [22], leading to uniform elongations that are lower than the HIP-underwent material. It is also interesting to note that all dual-phase microstructures lead to a smooth elasto-plastic transition with an initial hardening rate that is larger than that of the HIP-underwent microstructures. Even more interesting is the hardening behavior of samples annealed and quenched from lower temperatures (i.e. 920°C, 900°C and 850°C). In that case, the work-hardening rate is higher than that of the as-built part over the entire straining range, leading to larger ductilities simultaneously with higher stress levels. The hardening capabilities are also reported in Table 2 by the parameter $\Delta\sigma$. It can be highlighted that the hardening capability of the specimen annealed at 900°C is almost three times larger than that of the HIP-underwent or wrought specimens.

It is well documented in the literature that the $\alpha'$ martensite and the $\alpha$ phases exhibit different mechanical behaviors, see for example [15]. Martensite is indeed known for its high yield strength and low ductility,

**Table 2.** Heat treatment and resulting average fraction of martensite, yield strength $\sigma_y$, engineering ultimate tensile strength (UTS) $R_m$, true UTS $\sigma_m$, uniform engineering strain $e_u$, reduction of area $A_r$ and difference between the true UTS and the yield strength $\Delta\sigma$. Tensile properties measured for a specimen of wrought Ti–6Al–4V are also reported.

| | Fraction of $\alpha'$ (%) | $\sigma_y$ (MPa) | $R_m$ (MPa) | $\sigma_m$ (MPa) | $\Delta\sigma$ (MPa) | $e_u$ (%) | $A_r$ (%) |
|---|---|---|---|---|---|---|---|
| Wrought | 0 | 875 | 954 | 1050 | 175 | 10 | / |
| HIP-underwent | 0 | 914 ± 20.1 | 971 ± 22.1 | 1056 ± 33.5 | 142 ± 55.6 | 8.8 ± 2.1 | 37.8 ± 10.9 |
| 850°C—WQ | 30 ± 4 | 688 ± 18.2 | 1008 ± 3.9 | 1106 ± 3.3 | 418 ± 21.5 | 9.7 ± 0.1 | 38.6 ± 3.0 |
| 900°C—WQ | 38 ± 2 | 745 ± 12.1 | 1042 ± 7.9 | 1161 ± 17.2 | 416 ± 29.3 | 11.4 ± 1.0 | 42.0 ± 3.4 |
| 920°C—WQ | 51 ± 1 | 825 ± 32.7 | 1073 ± 7.3 | 1186 ± 10.9 | 353 ± 43.6 | 11.3 ± 0.3 | 41.3 ± 10.9 |
| 950°C—WQ | 63 ± 1 | 926 ± 9.2 | 1140 ± 4.4 | 1210 ± 1.8 | 285 ± 11.0 | 6.2 ± 1.3 | 40.7 ± 3.5 |
| 980°C—WQ | 80 ± 2 | 939 ± 13.9 | 1192 ± 8.4 | 1243 ± 8.0 | 304 ± 21.9 | 4.3 ± 0.9 | 27.5 ± 3.0 |

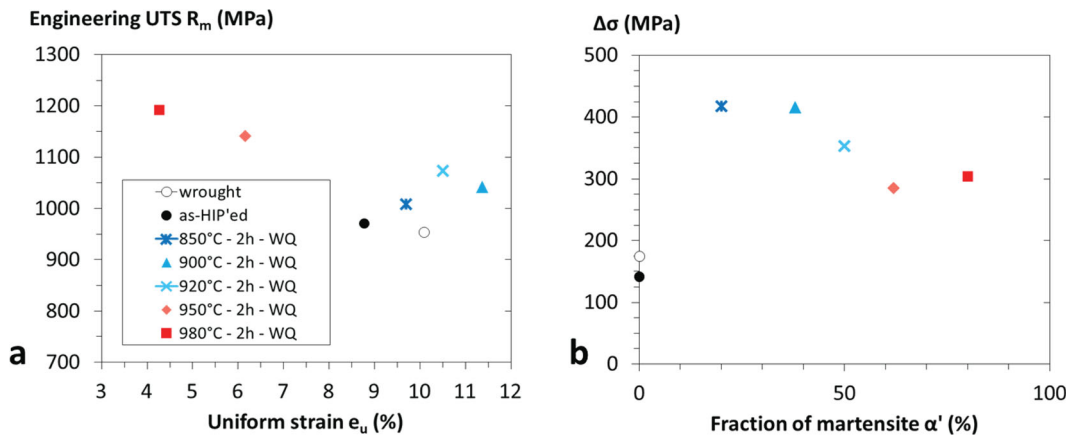


**Figure 5.** Engineering ultimate tensile strength $R_m$ as a function of the uniform strain (a) and difference between the true UTS and the yield strength $\Delta\sigma$ as a function of the fraction of martensite (b).

whereas the $\alpha$ phase exhibits a lower yield strength but a better ductility. This difference can clearly be observed when comparing the tensile curves of HIP-underwent specimens ($R_m = 970$ MPa; $A_r = 38\%$) to those of parts containing 80% of martensite ($R_m = 1192$ MPa; $A_r = 28\%$). The present results show that combining the two phases brings about a notable improvement in the mechanical behavior of the Ti–6Al–4V alloy. Not only is the strength/ductility balance improved, but a desirable work-hardening effect—rarely observed in Ti–6Al–4V [23]—is also achieved.

Such improved work-hardening capabilities can be ascribed to the heterogeneous multiphase microstructure developed during the heat treatment investigated in the present study. It is indeed well documented, since the seminal work of Ashby [24], that composite multiphase microstructures can lead to unexpected work-hardening properties when compared to their single-phase counterpart. This can be attributed to the difference in mechanical properties between the phases. Indeed, such a mechanical contrast leads to strain incompatibilities at the interfaces and to inhomogeneous deformation field that in turn translates into the building up of internal stresses. The internal stresses are accommodated by an important storage of geometrically necessary dislocations at the interfaces. Those additional dislocations participate to the global work-hardening behavior of the composite microstructure through the so-called kinematic hardening effect.

Such a synergy between a hard phase (here $\alpha'$) and a softer phase (here $\alpha$) has been reported and industrially used in the so-called Dual-Phase (DP) steels [25–27], especially in the automotive industry. Those steels consist of hard martensite and much softer ferrite [28–30]. They are also obtained through a similar heat-treatment process consisting of annealing within a two-phase region and fast cooling to room temperature. During quenching, DP steels and Ti–6Al–4V undergo a displacive phase transformation, leading to a dual-phase microstructure. Consequently, the literature on DP steels is particularly relevant to further enrich the discussion of the results obtained in this work. In DP steels, such as in Ti–6Al–4V, the two phases differ by their chemical composition that leads to a mechanical contrast between them. It should be noted, however, that this contrast is much more pronounced in DP steels because of the very important strengthening effect of the carbon in solid solution in the martensite [28–30].

In the case of the Ti–6Al–4V alloy, the work-hardening rate appears to be directly related to the volume fraction of $\alpha'$ martensite retained in the material. In the range of annealing temperatures investigated here, an optimum is obtained for a volume fraction of about 38%, that is, after performing a treatment at a temperature of 900°C. Indeed, at lower annealing temperatures, that is 850°C, although the hardening rate remains high, a decrease in uniform elongation is observed. It should be highlighted that the optimal fraction of martensite reported here is considerably larger than what is traditionally reported in DP steels [25–27]. This is most probably due to the fact that the mechanical contrast between the two phases in the present alloy is much less pronounced than in DP steels.

It should also be noted that a lower yield strength is observed in the specimens treated at lower annealing temperatures. A possible explanation for this decrease in yield strength might be the presence of soft orthorhombic $\alpha''$ martensite. Indeed, several authors report that orthorhombic $\alpha''$ martensite can form when quenching from annealing temperatures between 800°C and 900°C [3,16]. However, the XRD diffraction patterns (Figure 2) do not exhibit any distinct peak [31] highlighting the

presence of $\alpha''$. Therefore, although small amounts of $\alpha''$ martensite might be present, it is not believed that they would significantly impact the mechanical properties.

The low yield strength observed for lower annealing temperatures might be a direct consequence of the transformation strain associated to the $\beta \rightarrow \alpha'$ martensitic transformation. It might indeed lead to the formation of free dislocations within the $\alpha$ matrix. This behavior is also well known in DP steels [32]. This hypothesis requires additional investigations that go beyond the scope of this study.

## 4. Conclusions

The heat treatments investigated in this work generate much improved mechanical properties for additively manufactured parts made of Ti–6Al–4V. This can be attributed to a work-hardening behavior very rarely reported for this grade. A broad range of tensile properties can be obtained by playing with the $\alpha/\alpha'$ phase ratio. In addition, it should be highlighted that a remarkable improvement of the strength–ductility balance can be achieved. This distinctive tensile behavior and associated work-hardening might result in enhanced fatigue behavior or energy absorption capacities of additively manufactured parts. Further work includes evaluating the influence on the mechanical properties of the size and morphology of the $\alpha$ grains, which depend on the annealing time. Similar treatments should also be experimented on bimodal or equiaxed microstructures, that is, on forged Ti–6Al–4V.

## Disclosure statement

No potential conflict of interest was reported by the authors.

## Funding

The authors are grateful to the F.R.I.A. – F.N.R.S. for financing this research. The authors wish to acknowledge the Centre of Excellence of Multifunctional Architectured Materials 'CEMAM' n°AN-10-LABX-44-01 funded by the 'Investments for the Future' Program for having supported the stay of Pr. Stéphane Godet in Grenoble.

## References

[1] Lütjering G, Williams JC. Titanium. 2nd ed. Berlin, Germany: Springer; 2007.
[2] Leyens C, Peters M. Titanium and titanium alloys: fundamentals and applications. Weinheim, Germany: Wiley-VCH; 2003.
[3] Boyer R, Welsch G, Collings EW. Materials properties handbook: titanium alloys. Materials Park, OH: ASM International; 1994.
[4] Al-Bermani SS, Blackmore ML, Zhang W, et al. The origin of microstructural diversity, texture, and mechanical properties in electron beam melted Ti–6Al–4V. Metall Mater Trans A. 2010;41(13):3422–3434.
[5] Safdar A, Wei LY, Snis A, et al. Evaluation of microstructural development in electron beam melted Ti–6Al–4V. Mater Charact. 2012;65:8–15.
[6] Kobryn PA, Semiatin SL. Microstructure and texture evolution during solidification processing of Ti–6Al–4V. J Mater Process Technol. 2003;135(2):330–339.
[7] Wu X, Liang J, Mei J, et al. Microstructures of laser-deposited Ti–6Al–4V. Mater Des. 2004;25(2):137–144.
[8] Qian L, Mei J, Liang J, et al. Influence of position and laser power on thermal history and microstructure of direct laser fabricated Ti–6Al–4V samples. Mater Sci Technol. 2005;21(5):597–605.
[9] Antonysamy AA, Meyer J, Prangnell PB. Effect of build geometry on the $\beta$-grain structure and texture in additive manufacture of Ti6Al4V by selective electron beam melting. Mater Charact. 2013;84:153–168.
[10] de Formanoir C, Michotte S, Rigo O, et al. Electron beam melted Ti–6Al–4V: microstructure, texture and mechanical behavior of the as-built and heat-treated material. Mater Sci Eng A. 2016;652:105–119.
[11] Thijs L, Verhaeghe F, Craeghs T, et al. A study of the microstructural evolution during selective laser melting of Ti–6Al–4V. Acta Mater. 2010;58(9):3303–3312.
[12] Murr LE, Quinones SA, Gaytan SM, et al. Microstructure and mechanical behavior of Ti–6Al–4V produced by rapid-layer manufacturing, for biomedical applications. J Mech Behav Biomed Mater. 2009;2(1):20–32.
[13] Vrancken B, Thijs L, Kruth JP, et al. Heat treatment of Ti6Al4V produced by selective laser melting: microstructure and mechanical properties. J Alloys Compds. 2012;541:177–185.
[14] Qiu C, Adkins NJE, Attallah MM. Microstructure and tensile properties of selectively laser-melted and of HIPed laser-melted Ti–6Al–4V. Mater Sci Eng: A. 2013;578:230–239.
[15] Rafi HK, Karthik NV, Gong H, et al. Microstructures and mechanical properties of Ti6Al4V parts fabricated by selective laser melting and electron beam melting. J Mater Eng Perform. 2013;22(12):3872–3883.
[16] Vilaro T, Colin C, Bartout JD. As-fabricated and heat-treated microstructures of the Ti–6Al–4V alloy processed by selective laser melting. Metall Mater Trans A. 2011;42(10):3190–3199.
[17] Sun YY, Gulizia S, Oh CH, et al. The influence of as-built surface conditions on mechanical properties of Ti–6Al–4V additively manufactured by selective electron beam melting. JOM. 2016;68(3):791–798.
[18] Lu SL, Tang HP, Ning YP, et al. Microstructure and mechanical properties of long Ti–6Al–4V rods additively manufactured by selective electron beam melting out of a deep powder bed and the effect of subsequent hot isostatic pressing. Metall Mater Trans A. 2015;46:3824–3834.
[19] Castro R, Seraphin L. Contribution à l'étude métallographique et structurale de l'alliage de titane TA6V. Mém Sci Rev Mét. 1966;63(12):1025–1058.
[20] Matsumoto H, Yoneda H, Sato K, et al. Room-temperature ductility of Ti–6Al–4V alloy with $\alpha'$ martensite microstructure. Mater Sci Eng A. 2011;528:1512–1520.
[21] Tan X, Kok Y, Toh WQ, et al. Revealing martensitic transformation and $\alpha/\beta$ interface evolution in electron beam

melting three-dimensional printed Ti–6Al–4V. Sci Rep. 2016;6.
[22] Sachdev A. Effect of retained austenite on the yielding and deformation behavior of a dual phase steel. Acta Metall. 1983;31(12):2037–2042.
[23] Gupta RR, Anil Kumar V, Mathew C, et al. Strain hardening of titanium alloy Ti6Al4V sheets with prior heat treatment and cold working. Mater Sci Eng A. 2016;662:537–550.
[24] Ashby MF. The deformation of plastically non- homogeneous materials. Philos Mag. 1970;21(170):399–424.
[25] Davenport AT, editor. Formable HSLA and dual-phase steels. Proceedings. Warrendale (PA): TMS-AIME; 1979.
[26] Kot RA, Morris JW, editors. Structure and properties of dual-phase steels. Proceedings. Warrendale (PA): TMS-AIME; 1979.
[27] Kot RA, Bramfitt BL, editors. Fundamentals of dual-phase steels. Proceedings. Warrendale (PA): TMS-AIME; 1981.
[28] Tasan CC, Diehl M, Yan D, et al. Integrated experimental–simulation analysis of stress and strain partitioning in multiphase alloys. Acta Mater. 2014;81:386–400.
[29] Tasan CC, Hoefnagels JPM, Diehl M, et al. Strain localization and damage in dual phase steels investigated by coupled in-situ deformation experiments and crystal plasticity simulations. Int J Plasticity. 2014;63:198–210.
[30] Yan D, Tasan CC, Raabe D. High resolution in situ mapping of microstrain and microstructure evolution reveals damage resistance criteria in dual phase steels. Acta Mater. 2015;96:399–409.
[31] Zeng L, Bieler TR. Effects of working, heat treatment, and aging on microstructural evolution and crystallographic texture of $\alpha$, $\alpha'$, $\alpha''$ and $\beta$ phases in Ti–6Al–4V wire. Mater Sci Eng A. 2005;392:403–414.
[32] Rizk A, Bourell DL. Dislocation density contribution to strength of dual-phase steels. Scr Metall. 1982;16: 1321–1324.